Available online at www.sciencedirect.com
ScienceDirect
Biochimica et Biophysica Acta 1767 (2007) 79–87
Biochimica et Biophysica Acta
BBA
www.elsevier.com/locate/bbabio

Function of two β-carotenes near the D1 and D2 proteins in photosystem II dimers

Hiroshi Ishikita [a,c,*], Bernhard Loll [a], Jacek Biesiadka [a], Jan Kern [b], Klaus-Dieter Irrgang [b], Athina Zouni [b], Wolfram Saenger [a], Ernst-Walter Knapp [a,*]

[a] Institute of Chemistry and Biochemistry/Crystallography, Free University of Berlin, Takustrasse 6, D-14195 Berlin, Germany
[b] Max-Volmer-Laboratorium, Technical University of Berlin, Strasse des 17. Juni 135, D-10623 Berlin, Germany
[c] Department of Chemistry, The Pennsylvania State University, 104 Chemistry Building, University Park, PA 16802, USA

Received 10 August 2006; received in revised form 11 October 2006; accepted 12 October 2006
Available online 18 October 2006

Abstract

The antenna proteins in photosystem II (PSII) not only promote energy transfer to the photosynthetic reaction center (RC) but provide also an efficient cation sink to re-reduce chlorophyll *a* if the electron transfer (ET) from the Mn-cluster is inhibited. Using the newest PSII dimer crystal structure (3.0 Å resolution), in which 11 β-carotene molecules (Car) and 14 lipids are visible in the PSII monomer, we calculated the redox potentials (E_m) of one-electron oxidation for all Car (E_m(Car)) by solving the Poisson–Boltzmann equation. In each PSII monomer, the D1 protein harbors a previously unlocated Car (Car_{D1}) in van der Waals contact with the chlorin ring of $Chl_{Z(D1)}$. Each Car_{D1} in the PSII dimer complex is located in the interface between the D1 and CP47 subunits, together with another four Car of the other PSII monomer and several lipid molecules. The proximity of Car bridging between Car_{D1} and plastoquinone/Q_A may imply a direct charge recombination of $Car^{+}Q_A^{-}$. The calculated E_m(Car_{D1}) and E_m($Chl_{Z(D1)}$) are, respectively, 83 and 126 mV higher than E_m(Car_{D2}) and E_m($Chl_{Z(D2)}$), which could explain why Car^{+}_{D2} and $Chl^{+}_{Z(D2)}$ are observed rather than the corresponding Car^{+}_{D1} and $Chl^{+}_{Z(D1)}$.

Keywords: Photosystem II; Chlorophyll; β-carotene; Photoprotection; Electron transfer; Redox potential

1. Introduction

The initiation of electron transfer (ET) in the photosynthetic reaction center (RC) of photosystem II (PSII) depends strongly on efficient population of the electronic excited state of P680. It was suggested [1] that the chlorophyll *a* (Chl*a*) in the antenna complexes CP43 and CP47 participate in energy transfer to the RC (Fig. 1a). In functionally impaired PSII, the positive charge (electron hole) localized at the cation radical $P680^{+\bullet}$ as a result of charge separation is not transferred to the Mn-cluster. Especially if tyrosine Y_Z is unable to reduce $P680^{+\bullet}$, because of loss of redox activity at low temperatures or a missing Mn-cluster, the population of the state $P680^{+\bullet}$ can be built up in such functionally impaired PSII. As a consequence, triplet states of the Chl*a* may form in the RC and lead finally to singlet oxygen, which can damage the PSII complex. According to recent studies, P680 probably consists of the Chl*a* from the $P_{D1/D2}$ pair and of the accessory Chl*a* ($Chl_{D1/D2}$), which result from the charge separation process. Subsequently, the cationic state moves from the initial electron donor, $Chl_{D1/D2}$, to the $P_{D1/D2}$ pair that serves as electron acceptor for the Mn-cluster (reviewed in ref. [2]).

Abbreviations: β-DM, *n*-dodecyl-β-D-maltoside; Car, β-carotene; $Chl_{D1(D2)}$, accessory Chl*a* in D1(D2); Chl*a*, chlorophyll *a*; $Chl_{Z(D1(D2))}$, chlorophyll $_Z$ in D1(D2); cyt b_{559} (c_{550}), cytochrome b_{559} (c_{550}); DGDG, digalactosyl diacyl glycerol; E_m, (midpoint) redox potential; ET, electron transfer; LPB equation, linearized Poisson–Boltzmann equation; MGDG, monogalactosyl diacyl glycerol; Mn-cluster, oxygen-evolving complex with Mn ions; Mn-depleted PSII, PSII with depleted Mn-cluster; NHE, normal hydrogen electrode; P680, Chl*a* of PSII RC absorbing at 680 nm; $Pheo_{D1(D2)}$, pheophytin *a* in D1(D2); PSII, photosystem II; $Q_{A(B)}$, plastoquinone in A(B)-branch; RC, reaction center; SQDG, sulfoquinovosyl diacylglycerol

* Corresponding authors. H. Ishikita is to be contacted at Tel.: +1 814 865 2120; fax: +1 814 863 5319. E.W. Knapp, tel.: +49 30 83854387; fax: +49 30 83856921.
E-mail addresses: hzi1@psu.edu (H. Ishikita), knapp@chemie.fu-berlin.de (E.-W. Knapp).

0005-2728/$ - see front matter © 2006 Elsevier B.V. All rights reserved.
doi:10.1016/j.bbabio.2006.10.006

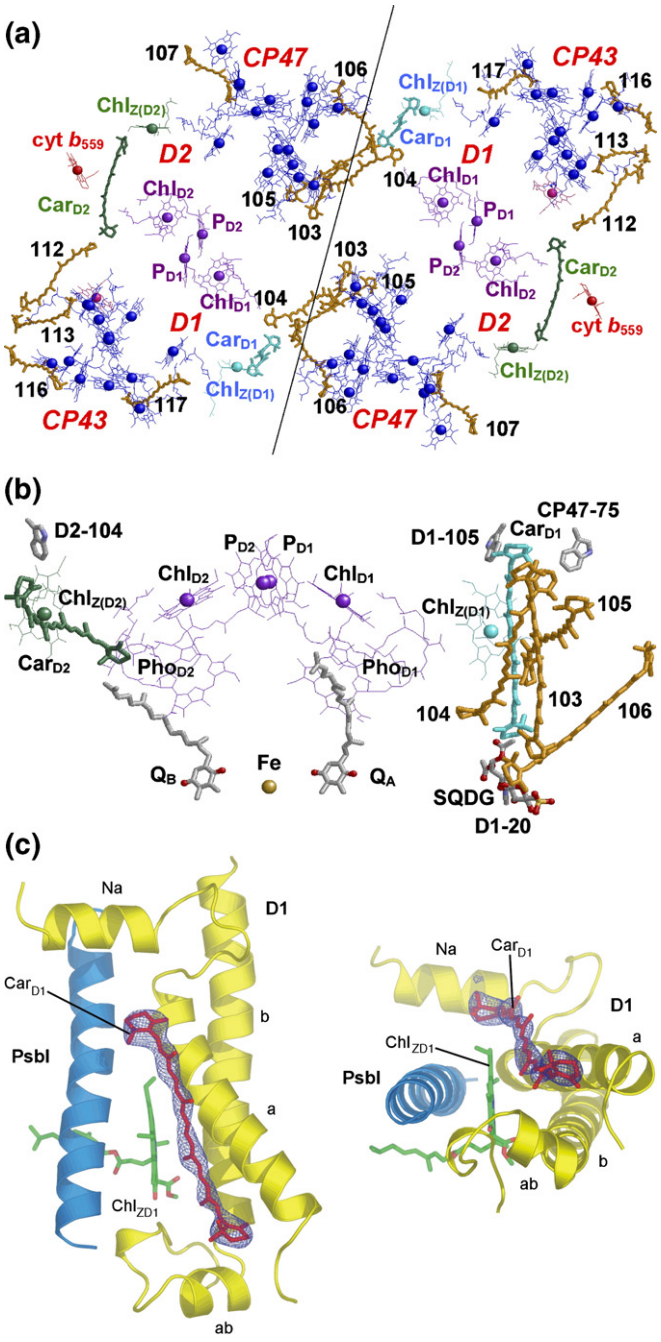

Fig. 1. (a) Location of Car and Chl*a* in the PSII dimer. Car_{D1} and $Chl_{Z(D1)}$ are colored in cyan while Car_{D2} and $Chl_{Z(D2)}$ are colored in green. The other Chl*a* in antenna complex, RC and Car are colored in blue, purple and orange, respectively. The monomer–monomer interface is indicated as solid line. (b) Location of Car_{D1} (cyan) in the cluster of four Car (orange) with respect to RC. (c) Electron density map of Car_{D1} from the PSII crystal structure at 3.0 Å resolution. (For interpretation of the references to colour in this figure legend, the reader is referred to the web version of this article.)

β-carotene (Car) and antenna Chl*a* play an important role in avoiding this damage by means of ET to $P680^{+\bullet}$ [3–5]. In the corresponding ET pathway, a Car molecule near $Chl_{Z(D2)}$ (Car_{D2}) is an initial electron donor to $P680^{+\bullet}$, and the donor to Car^{+}_{D2} is either cytochrome (cyt) b_{559} or $Chl_{Z(D2)}$ when cyt b_{559} is in the reduced (cyt b^{0}_{559}) or oxidized state (cyt b^{+}_{559}), respectively [4,5]. On the other hand, the proposed existence of the corresponding Car in or near the D1 protein (Car_{D1}) was based mainly from IR spectroscopic studies that identified two clearly distinguishable Car_{489} and Car_{507}. The former absorbs in the visible at 489, 458 and 429 nm while the latter absorbs at 507, 473 and 443 nm [6–11]. Tomo et al. proposed that Car_{489} and Car_{507} are Car_{D1} and Car_{D2}, respectively [8]. Two redox-active Car were also observed in a recent resonance Raman study of PSII core complex [12]. Direct electrochemical measurements of the redox potential for these Car in PSII could elucidate their capability as oxidants, but coexistence of several other redox cofactors renders such a determination impossible (reviewed in ref. [13]).

Biochemical analysis for *Synechocystis* PCC 6803 PSII revealed 14 Car [13] or 11±1 Car [14]. The number of Car molecules assigned in former PSII crystal structures is smaller. In the 3.8 Å resolution structure no Car could be assigned and orientations of Chl*a* were unclear [15]. In another 3.7 Å resolution structure two Car were assigned on the D2 side [16]. Their configuration, however, is a matter of debate, as one of them was modeled as *cis* configuration, which is in contradiction to spectroscopic data [12]. The 3.5 Å resolution structure contains the two Car [17] at about the same positions (but *trans* in configuration) as observed in the 3.7 Å resolution structure. In the present crystal structure at 3.0 Å resolution from *Thermosynechococcus elongatus* (*T. elongatus*), 11 Car have been revealed per PSII monomer [18] (Fig. 1a). This agrees with a recent biochemical evaluation of PSII composition that identified 9±1 Car per *T. elongatus* PSII monomer [19]. The variation of the number of Car found in PSII may depend on the method or may be due to differences in species. The stringent purification methods used for crystallization may yield a smaller number of Car found in PSII. Recent X-ray absorption spectroscopic studies on radiation damage to PSII deals in particular with changes occurring at the Mn-cluster [20]. Even though possible damage to Chl*a*, Car or other amino acid sidechains cannot be excluded, they were not observed. Radiation damage is a common problem in structural biology and most likely occurs at amino acids exposed to solvent, disulfide bridges and metal centers. But PSII is unlikely to lose cofactors upon exposure to X-rays [18]. The reason why the Mn-cluster is ill-defined in the apparent electron density of PSII crystals may be related to their high flexibility, which promotes conformational disorder.

The level of refinement of the present 3.0 Å structure is far higher than that of other structures currently available for PSII. There are 63639 unique reflections for the 3.8 Å structure [15], whereas for the 3.5 Å structure [17] there are 103604. The present 3.0 Å PSII structure is based on an even larger number (155380) of unique reflections, [18]. This increased number of reflections results in a much better data-to-parameter ratio and allows a more reliable refinement, which yields small errors in the atomic coordinates. Thus, for the purpose of exploring the energetics of Car in PSII the present crystal structure *T. elongatus* PSII is an appropriate starting point. Here, we report redox potentials (E_m) for one-electron oxidation of all 11 Car (E_m(Car)) of PSII, focusing mainly on a newly found Car at the D1 side and another Car at the D2 side.

2. Methods

2.1. Coordinates

Atomic coordinates were taken from the crystal structure of dimeric PSII from *T. elongatus* at 3.0 Å resolution (PDB: 2AXT) [18], obtained by further refinement of the previous structure at 3.2 Å resolution (PDB, 1W5C) [21]. Hydrogen atoms were placed in energy-optimized positions with CHARMM [22]. A membrane of lipid molecules with thickness ~20 Å was explicitly generated around the PSII dimer in order to mimic the thylakoid membranes (see Supplementary Discussion).

2.2. Atomic partial charges

The same atomic partial charges as in our previous computations were used [23]. Specifically, we used the same atomic charges for Chl*a* and His-ligated Chl*a* (for $P_{D1/D2}$ and $Chl_{Z(D1/D2)}$) as in previous studies [23]. The atomic charges of phospholipid 1,2-dipalmitoyl-phosphatidyl-glycerole (PG) are given in Ref. [24]. The atomic charges of the newly found lipids (digalactosyl diacyl glycerol (DGDG), monogalactosyl diacyl glycerol (MGDG), sulfoquinovosyl diacylglycerol (SQDG)) and detergent molecules (*n*-dodecyl-β-$_D$-maltoside (β-DM)) were determined from the electronic wave functions by fitting the resulting electrostatic potential in the neighborhood of these molecules by the RESP procedure (Supplementary Table S1–4) [25]. The electronic wave functions were calculated with JAGUAR [26] using the 6-31G* basis set. The charges for the β-carotene molecules and the phytol chain of the Chl*a*, Pheo*a*, quinones, lipids and detergent molecules were assigned a standard charge of +0.09 for non-polar hydrogen atoms and vanishing total charge for each CH_n group as for analogous cases in the CHARMM22 parameter set [27]. The same procedure was used in previous computations [23]. Computations were done for Mn-cluster charges corresponding to the S_1 state (for charges, see ref. [23]) if not otherwise specified. Those computations were based on numerical solutions of the linearized Poisson–Boltzmann (LPB) equation with the program MEAD [28].

2.3. Mn-depleted PSII model

Most of the experimental studies on Car cation radicals in PSII (for instance, [5]) have been done on Mn-cluster depleted preparations (Mn-depleted PSII). A corresponding crystal structure is not available yet. Although the Mn-depleted PSII samples could be subject to critical changes in conformation or H-bond network compared with the intact PSII (see for instance Refs. [29,30]), we neglected geometry changes and just removed the Mn and Ca ions to estimate the E_m of the Mn depleted PSII. In the presence of the Mn-cluster the titratable Mn-cluster ligands were fixed in their deprotonated states. These ligands are the negatively charged acidic residues (D1-Asp170, D1-Glu189, D1-Glu333, D1-Asp342, CP43-Glu354, and C-terminal backbone carboxylic group of D1-Ala344) and the uncharged D1-His332. In the Mn-depleted PSII model these ligating residues are free to be protonated. Hence, the protonation states of these residues were fully titrated and equilibrated.

2.4. Reference model system for Car

To obtain the absolute value of E_m in the corresponding protein environment, we calculated the electrostatic energy difference between the two redox states of Car or Chl*a* in a reference model system. The calculated shift of E_m in the protein relative to the reference system was added to the experimental E_m value. As a reference model system, the following E_m for one-electron oxidation in solution *versus* normal hydrogen electrode can be used: E_m^{water} (Car)=+782 mV in water [31] or E_m^{CH2Cl2} (Car)=+897 mV in CH_2Cl_2 [32]. Electrolyte and aprotic solvent used in electrochemical measurements can affect the measured E_m. Using CH_2Cl_2 with ε=9 as a model reference system, we calculated $E_{m,theory}^{water}$ (Car)−$E_{m,theory}^{CH2Cl2}$ (Car)=−145 mV from electrostatic energies. This yields an $E_{m,theory}^{water}$ (Car)=+752 mV close to $E_{m,experiment}^{water}$ (Car)=+782 mV [31] (i.e., the computed E_m varies by only 30 mV with the choice of the reference model system). As in previous computations [33], we used $E_{m,experiment}^{water}$ (Car)=+782 mV. Thus, the electrostatic approach of the present study provides consistent results for the E_m computations.

2.5. Reference model system for Chla

For one-electron oxidation E_m(Chl*a*) was measured in different solvents (reviewed in ref. [34]). As in previous studies [23], we consider those measured in CH_2Cl_2 because the inability of CH_2Cl_2 to ligate to Mg^{2+} of Chl*a* does not affect E_m by changes in solvation and electronic energy, in contrast to acetonitrile or tetrahydrofuran where ligation of solvent molecules is possible (reviewed in ref. [34]).

E_m(Chl*a*) was measured to be +800 mV (versus normal hydrogen electrode) in CH_2Cl_2 [35,36]. Taking into account the solvation energy difference between CH_2Cl_2 and water, we used the value of +698 mV as a reference E_m for Chl*a* in water [23]. We evaluated the influence of a His ligand on E_m for Chl*a* in water and used E_m(Chl*a*)=+585 mV as a reference [23].

2.6. Computation of E_m

The ensemble of protonation patterns was sampled by a Monte Carlo method with our own program Karlsberg (Rabenstein, B. *Karlsberg online manual*, http://agknapp.chemie.fu-berlin.de/karlsberg/ (1999)). The dielectric constant was set to ε_P=4 inside the protein and ε_W=80 for water, as in previous computations (for instance, [23]). All computations were performed at 300 K with pH 7.0 and an ionic strength of 100 mM. In general, the dielectric constant is temperature-dependent. For instance, ε_W=80 is the value experimentally obtained for water at room temperature. On the other hand, ε_P is an empirically evaluated dielectric constant for the protein, being used jointly with ε_W=80. Although the values of ε_P used in some electrostatic computations lie between 2 and 20 [37], we uniformly used the combination of ε_P=4 and ε_W=80 to calculate E_m or pK_a at room temperature. Though in PSII Car^+ and Chl_Z^+ can be measured at low temperatures [5,38], we have not established the validity of ε_P at those temperatures with a corresponding ε_W. In addition, we need values of reference models to calculate E_m (i.e. E_m values for reference redox-active groups) and the protonation pattern (i.e. pK_a values for reference titratable groups). Corresponding values are generally not available. Because of a lack of information we calculated E_m for redox-active groups and protonation states for titratable residues only at 300 K. Nevertheless, we believe that calculating E_m for each redox group and titratable group in PSII at 300 K provides data that complement experiments.

The LPB equation was solved using a three-step grid-focusing procedure with 2.5 Å, 1.0 Å and 0.3 Å resolutions. The Monte Carlo sampling yielded probabilities [A_{ox}] and [A_{red}] of the two redox states of molecule *A*. The E_m were evaluated from the Nernst equation. A bias potential was applied to obtain equal probabilities for both redox states ([A_{ox}]=[A_{red}]), yielding the redox midpoint potential E_m as the bias potential. For convenience, the computed E_m were given with mV accuracy, without implying that the last digit is significant. For further information about the E_m computation and error estimate, see ref. [23].

3. Results and discussion

3.1. Car_{D1} is Car_{489}

In the present PSII crystal structure [18], the Car near $Chl_{Z(D1)}$ (Car-101, termed Car_{D1}) is approximately perpendicular to the membrane plane while the Car near Chl_{D2} and $Chl_{Z(D2)}$ (Car-111, termed Car_{D2}) is nearly parallel to the membrane plane, in agreement with Car_{489} and Car_{507}, respectively, proposed from previous spectroscopic studies [6–8]. Fig. 1c shows the electron density map of Car in PSII. Atomic positions within Car's are determined reliably (Fig. 1c). Both Car are at a center-to-center distance of about 36 Å from the non-heme iron in the RC, which is similar to the distance of 38 Å indicated by EPR studies [39], and both Car_{D1} and Car_{D2} are in the all-*trans* configuration, in agreement with the results of a recent resonance Raman spectroscopic study [12]. Car_{D1} and $Chl_{Z(D1)}$ are both near the PSII monomer-monomer interface. The rather

hydrophobic environment of Car_{D1} surrounded by several lipid molecules and another four Car molecules (Car-103, 104, 105 and 106) contrasts with that of Car_{D2} whose neighborhood contains only one other Car (Car-112) and fewer lipid molecules.

3.2. Electron transfer from cyt b_{559} to $P680^{+\bullet}$

The spectroscopically identified Car_{D2} was recently suggested to participate in ET from cyt b^0_{559} to $P680^{+\bullet}$ [5] (Fig. 2, Scheme 1). This agrees with the PSII crystal structures where cyt b_{559} is closer to Car_{D2} than to Car_{D1} [17,18]. The measured E_m of +390 mV for cyt b_{559} in its high-potential form [40] is sufficiently low to reduce Car. The formation of Car^+ or Chl^+_Z can be observed only in the presence of oxidized cyt b_{559} (i.e., they are easily reduced by reduced cyt b_{559}). In PSII from spinach, Car^+ is detected only at low temperatures (20 K), while Chl^+_Z is predominantly observed at elevated temperatures (120 K) [5]. In PSII from *Synechocystis* PCC 6803 both Car^+ and Chl^+_Z can be photo-accumulated at 20 K [38].

In PSII from *Synechocystis* PCC 6803, the redox-active Chl_Z involved in cation quenching was identified from EPR and Raman studies as $Chl_{Z(D1)}$ ligated by D1-His118 [38]. In contrast, measurements of fluorescence emission spectra of PSII from *Chlamydomonas reinhardtii* pointed to $Chl_{Z(D2)}$ as the ET-active Chl_Z [41]. According to near-IR studies, both $Chl_{Z(D1)}$ and $Chl_{Z(D2)}$ can be photo-oxidized in PSII from spinach [42]. EPR studies on the other hand suggested that $Chl_{Z(D2)}$ was the photo-oxidized Chl_Z in spinach PSII [43]. In a previously determined PSII crystal structure, one Chl*a* (Chl*a*-47) was found at 18 Å (center-to-center distance) from $Chl_{Z(D1)}$ [17]. Based on this crystal structure, the calculated E_m(Chl*a*-47) is at the same level as that of the neighboring Chl*a*, $Chl_{Z(D1)}$ and Chl*a*-18 (ligated by CP43-His430) [33]. Therefore, we proposed that the $Chl^+_{Z(D1)}$ state could be formed by electron-hole transfer via these antenna Chl*a* in CP43 [33], as was originally proposed in a theoretical study by Vasil'ev et al. [44].

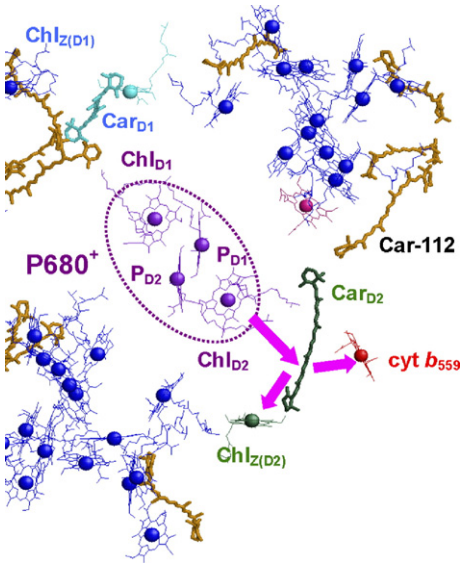

Fig. 2. Electron hole transfer pathway via Car_{D2}.

cyt b_{559} ↘
Chl$_{Z(D2)}$ ↗ Car$_{D2}$ → P680

Scheme 1.

However, in the present crystal structure at higher resolution [18] there is a lipid molecule (DGDG-2) at the location of Chl*a*-47 that cannot be oxidized. Thus, the participation of alternative redox-active cofactors for electron-hole transfer in the antenna complex seems to be required. There is no doubt about the lipid at this location, as the binding pocket for Chl*a* and the head group of a lipid molecule differ significantly [18].

In the present study based on the new PSII crystal structure, the calculated $E_m(Car_{D1})$ and $E_m(Chl_{Z(D1)})$ are +997 mV and +837 mV, respectively (Table 1) in the dimer form of the PSII structure (note: the E_m are calculated for the PSII dimer form, if not specified otherwise). On the other hand, the calculated E_m (Car_{D2}) and $E_m(Chl_{Z(D2)})$ are +914 mV and +711 mV, respectively. The lower E_m values for Car and Chl_Z on the D2 side imply that Car and Chl_Z could oxidize preferentially on the D2 side, as opposed to the D1 side. Furthermore, an $E_m(Chl_{Z(D2)})$ lower than $E_m(Car_{D2})$ could explain why $Chl^+_{Z(D2)}$ is predominantly observed (with respect to Car^+_{D2}) at elevated temperatures (120 K) [5].

Oxidation of Chl_Z or Car on the D2 side is energetically advantageous, since cyt b_{559} is sufficiently close to permit their re-reduction (Fig. 1a). Although the formation of Chl^+_Z and Car^+ can be observed only in the presence of pre-oxidized cyt b_{559} [5], the change in the redox state of cyt b_{559} only slightly affects the calculated $E_m(Chl_{Z(D2)})$ and $E_m(Car_{D2})$ by up to ~20 mV (Table 1, blue numbers).

Table 1
Calculated E_m(Chl*a*) and E_m(Car) in the PSII dimer form

Cofactors	Charge states of individual cofactors	
Chl*a*/Car [a]	Neutral	Other states [b]
P_{D1}	+1206	
P_{D2}	+1222	
Chl_{D1}	+1262	
Chl_{D2}	+1320	
$Chl_{Z(D1)}$	+837	+964 (Car^+_{D1}), +837 (cyt b^+_{559})
$Chl_{Z(D2)}$	+711	+733 (Car^+_{D2}), +719 (cyt b^+_{559})
101 (Car_{D1})	+997	+1122 ($Chl^+_{Z(D1)}$), +997(cyt b^+_{559})
111 (Car_{D2})	+914	+938 ($Chl^+_{Z(D2)}$), +937(cyt b^+_{559})
Car-103	+1043	
Car-104	+1005	
Car-105	+1124	
Car-106	+971	
Car-107	+847	
Car-112	+955	
Car-113	+991	
Car-116	+866	
Car-117	+963	

[a] The numbering is consistent with that of the original crystal structure and Fig. 1a.
[b] For E_m values calculated in the P^+_{D1}, Chl^+_{D1} and Q^-_A states, see supplementary Table S6.

Between the D1 and D2 sides there are also differences of the interaction between Chl_Z and Car in their oxidized (charged) states. On the D2 side, oxidation of Car_{D2} and $Chl_{Z(D2)}$ has negligible influences on $E_m(Chl_{Z(D2)})$ and $E_m(Car_{D2})$, respectively (Table 1, blue numbers), while oxidation of Car_{D1} and $Chl_{Z(D1)}$ shifts $E_m(Chl_{Z(D1)})$ and $E_m(Car_{D1})$ up by ~130 mV (Table 1, red numbers). Fig. 1a shows that the chlorin of $Chl_{Z(D2)}$ is at one end of the Car_{D2} "wire" (Fig. 1a) while that of $Chl_{Z(D1)}$ is in van der Waals contact with Car_{D1} in the center of the Car wire (edge-to-edge distance 3.7 Å and π–π distance 4.1 Å) (Fig. 1b). The closer contact of $Chl_{Z(D1)}$ with Car_{D1} is probably the reason for the strong mutual electrostatic response when a positive charge is localized at $Chl_{Z(D1)}$ or Car_{D1}. As a consequence, the positive charge is probably delocalized over $Chl_{Z(D1)}$ and Car_{D1}, although this delocalization might be specific to spinach PSII [42] and not apply to PSII from cyanobacteria [18].

3.3. Mn-cluster and protonation states of residues influencing E_m(Car)

One of the significant structural differences between the D1 and D2 sides is that the former is involved in the PSII monomer–monomer interface (Fig. 1a), which may induce differences in E_m(Car). Indeed, upon monomerization of PSII the calculated $E_m(Car_{D1})$ is significantly reduced from +997 mV to +931 mV, while the calculated $E_m(Car_{D2})$ remains essentially unchanged (+914 mV for dimer PSII and +899 mV for monomer PSII including the influence of the membrane, see supplementary Table S5). Nevertheless, it should be noted that the protein dielectric volume (i.e. the space covered by the merged van der Waals volumes of protein atoms) does not discriminate between the E_m values for Car_{D1} and Car_{D2} even in PSII dimer form (Table 2). Therefore, we conclude that atomic charges in the PSII monomer–monomer interface, but not the protein dielectric volume, are responsible for the increase of the $E_m(Car_{D1})$ with respect to $E_m(Car_{D2})$. Contrary to $E_m(Car_{D1/D2})$, the calculated $E_m(Chl_{Z(D1/D2)})$ remain essentially unchanged (+834 mV/ +703 mV for $Chl_{Z(D1/D2)}$ including the membrane influence) in the isolated PSII monomer in spite of the proximity of $Chl_{Z(D1)}$ to Car_{D1}. (The chlorin of $Chl_{Z(D1)}$ is in van der Waals contact with Car_{D1}, the edge-to-edge distance is 3.7 Å and the π–π distance is 4.1 Å).

On the other hand, the present study indicates that the atomic charges of PSII shift $E_m(Car_{D1})$ and $E_m(Chl_{Z(D1)})$ upward by 69 mV and 104 mV with respect to $E_m(Car_{D2})$ and $E_m(Chl_{Z(D2)})$ (Table 2, last line). It is remarkable that the influence of cofactor charges on $E_m(Car_{D2})$ is exactly compensated by the charges of the protein, in contrast to the situation for $E_m(Car_{D1})$ (Table 2). Among the cofactors in PSII, the positively-charged Mn-cluster is responsible for the E_m increase of 71 mV in Car_{D1} and of 111 mV in $Chl_{Z(D1)}$ relative to Car_{D2} and $Chl_{Z(D2)}$, respectively (Table 2). Hence, the proximity of the Mn-cluster (S1 state) and insufficient compensation of its positive charge by protein charges in the D1 protein, as compared to the D2 protein, seem to be the main causes for the lowering of the E_m values of Car_{D2} and $Chl_{Z(D2)}$ with respect to Car_{D1} and $Chl_{Z(D1)}$.

To confirm this conclusion obtained from calculations for the S1 state, we also calculated E_m for the Mn-depleted PSII model. Note that in our previous computations a significant decrease of E_m for the redox-active tyrosine Y_Z (on the D1 side) was observed upon depletion of the Mn-cluster [45]. The calculated $E_m(Car_{D1/D2})$ and $E_m(Chl_{Z(D1/D2)})$ for the Mn-depleted PSII (Table 3) are, however, almost the same as those for the S1 state in presence of the Mn-cluster (Table 2). The lack of a shifts in E_m in the presence of the Mn-cluster is due to significant changes in protonation pattern of titratable residues that compensate for the loss of the positive charge at the Mn-cluster (see influence of protein sidechains in Table 3). In the present computation, the D1-His332 ligand of the Mn-cluster, being uncharged for the S1 state, becomes positively charged (fully protonated) upon depletion of the Mn-cluster. The Mn-cluster ligands D1-Glu333, D1-Asp342, CP43-Glu354 are fully deprotonated in the S1 state and mostly or fully protonated in the Mn-depleted PSII. Either D1-Glu189 or D1-Glu333, both Mn-cluster ligands, are likely to protonate upon depletion of the Mn-cluster, since we observed protonation of one of the two residues in each PSII monomer of the dimer complex. In proteins, acidic residues are often deprotonated, but on account of the unusual protein environment around the Mn-cluster with negatively charged ligands that stabilize the positively charged Mn-cluster (see also discussion in ref. [23]), protonation of

Table 2
Redox potentials (E_m) and contributions from different parts of PSII (ΔE_m) in the S1 state of the PSII dimer form

	$Chl_{Z(D1)}$	$Chl_{Z(D2)}$	Car_{D1}	Car_{D2}
E_m	837	711	997	914
E_m(uncharged)[a]	687	665	928	914
ΔE_m[b]	150	46	69	0
(a) Cofactor	156	27	106	63
(Mn-cluster)	131	20	110	39
(b) Protein	−6	19	37	−63
backbone	133	26	67	12
(backbone in D1/D2)	78	52	12	-5
sidechain	−139	−7	−104	−75

[a] E_m values calculated in protein dielectric volume in absence of atomic charges indicating that protein dielectric volume is mainly not responsible for the E_m difference of Chl_Z and Car between the D1 and D2 sides.
[b] $\Delta E_m = E_m$(charged) − E_m(uncharged).

Table 3
Redox potentials (E_m) and different contributions from different parts of PSII (ΔE_m) for the Mn-depleted PSII dimer form

	$Chl_{Z(D1)}$	$Chl_{Z(D2)}$	Car_{D1}	Car_{D2}
E_m	813	712	980	914
E_m(uncharged)[a]	687	665	928	914
ΔE_m[b]	126	47	52	0
(a) Cofactor	25	7	−4	24
(Mn-cluster)	0	0	0	0
(b) Protein	101	40	56	−24
backbone	133	26	67	12
sidechain	−32	14	−11	−36

[a] E_m values calculated in protein dielectric volume in absence of atomic charges, indicating that protein dielectric volume is mainly not responsible for the E_m difference of Chl_Z and Car between the D1 and D2 sides.
[b] $\Delta E_m = E_m$(charged) − E_m(uncharged).

some of these acidic residues is energetically favorable for the Mn-depleted PSII. As observed in comparable situations [46–48], conformational changes of side chains [29,30] may occur to compensate accumulated negative charges remaining after removal of the Mn-cluster. It is also notable that we observed only small changes in the pattern of protonation at D1-Asp59, D1-Glu65, D2-Glu312 and D2-Lys317. These residues have been suggested to form a possible proton exit pathway linked to water oxidation at the Mn-cluster [17,49–52]. Changes in their protonation states upon S-state changes have been demonstrated [52].

We conclude that asymmetric location of the Mn-cluster is ultimately responsible for the lower E_m values of Car_{D2} and $Chl_{Z(D2)}$ with respect to Car_{D1} and $Chl_{Z(D1)}$. The presence of the Mn-cluster with its positive charges has a significant influence on these E_m. In the absence of the Mn-cluster acidic residues, whose original function is to stabilize the positively charged Mn-cluster, become protonated and thus compensate the influence on these E_m resulting from the loss of positive charges.

3.4. Charge recombination of an unidentified Car^+ with Q^{A-}

Biphasic kinetics of irreversible bleaching indicated that one Car (presumably Car_{D2}) is more easily oxidized than the other [53]. As Car^+ is very short-lived in the presence of cyt b^0_{559}, Car^+_{D2} could not be trapped even at 20 K in PSII-enriched membranes [4]. However, oxidation of two Car (presumably Car_{D2} and another Car that we call "Car_X" in the following discussion) occurs approximately to the same extent in the PSII core complex [11] and PSII RC samples [10] either by charge separation at low temperatures or with the help of the exogenous electron acceptor SiMo (silicomolybdate). Two redox-active Car were also observed in a recent resonance Raman study of the PSII core complex [12]. FTIR studies suggested that Car_{D2} seems to be preferentially oxidized by $P680^{+\bullet}$ [54]. Under more *in-vivo* like conditions of PSII-enriched membrane samples [4], oxidation of Car_{D1} seems to be disfavored compared with that of Car_{D2}. Nevertheless, a low quantum yield oxidation of Car_{D1} may also occur, as suggested by Telfer [9].

In PSII enriched membranes only one cationic Car^+ was observed whereas two such Car^+ appear in PSII RC samples (D1-D2-cyt b_{559} sub-complex). This may result from the absence of Q_A in the latter case. In another isolated PSII sub-complex composed of D1, D2, cyt b_{559} and CP47 (CP47-RC), Q_A was found only in the CP47-RC dimer, but not in the monomer [55]. In this case, it was demonstrated that Q_A in CP47-RC dimer helps to slow down charge recombination processes involving $P680^{+\bullet}$ [56], thus lowering ^{3}P680 yield [57]. Charge recombination pathways involving $P680^{+\bullet}Pheo^-_{D1}$ dominate in wild type PSII and are known to generate ^{3}P680 [58]. Car cannot quench ^{3}P680, unless it is at van der Waals contact [59–61] (see Fig. 3). This suggests that the reduced susceptibility to photo-damage in the CP47-RC dimer can be attributed to the presence of Q_A [57], which slows charge recombination to $P680^{+\bullet}$ and thus diminishes ^{3}P680 yield.

Even in more complete PSII complexes that include Q_A (i.e., PSII enriched membranes) $P680^{+\bullet}Car^0_XQ^-_A$ may decay to the ground state via the intermediate $P680^0Car^+_XQ^-_A$ with low quantum yield. Indeed, a slightly lower quantum yield of 13% cyt b^+_{559}/Q^-_A, compared with 5% Car^+/Q^-_A in the PSII enriched membranes, was interpreted as charge recombination occurring, at least in part, via $P680^0Car^+Q^-_A$ [5]. If we consider that in PSII RC samples the occurrence of Car^+_X is very likely [10,11], then Car^+_{D1} may form transiently in the PSII enriched membranes, as previously suggested [9]. Nevertheless, it should be noted again that conversion of $P680^{+\bullet}Car^0_XQ^-_A$ to $P680^0Car^+_XQ^-_A$ probably occurs with low quantum yield because of the following: (i) relatively rapid $P680^{+\bullet}Car^0_XQ^-_A$ charge recombination (~100 μs [62]), which might occur directly or in two steps: a first slow process "$P680^+Car^0_XQ^-_A \rightarrow P680^0Car^+_XQ^-_A$", followed by faster

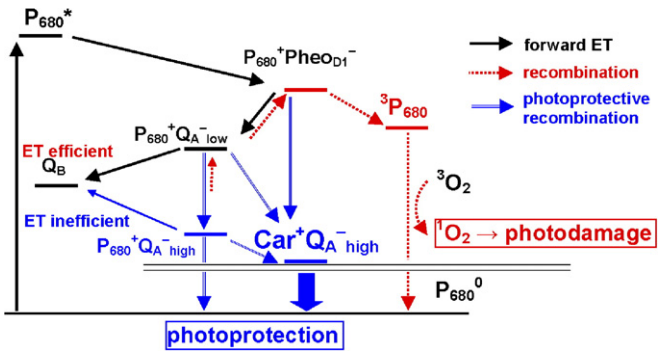

Fig. 3. Energetics of the forward and backward (charge recombination) ET processes in PSII.

process of "$P680^0Car_X^+Q_A^-$ charge recombination", (ii) a preferential oxidation of Car_{D2} [5,54], which is demonstrated in the present study (for a Car_X candidate, see discussion in the next section).

$E_m(Q_A)$ measurements of Krieger et al. indicated the existence of two PSII species with a difference of 145 mV in $E_m(Q_A)$, which suggests low-potential and a high-potential forms of Q_A [63,64]. The high-potential form of Q_A, which appears after deactivation of O_2 generation in PSII, results in a larger E_m difference between Q_A and $Pheo_{D1}$ than the low-potential form, which implies that charge recombination of $P680^{+\bullet}Q_A^-$ occurs directly without involving the intermediate state $P680^{+\bullet}Pheo_{D1}^-$ [58] (Fig. 3). The $P680^{+\bullet}Pheo_{D1}^-$ state is known to generate triplet states at P680 with high yield. Hence, in O_2-evolving active PSII with Q_A in the low-potential form, charge recombination of $P680^{+\bullet}Q_A^-$ seems to occur via $P680^{+\bullet}Pheo_{D1}^-$ [58] and the high-potential form of Q_A was proposed to be photo-protective [58,63,64]. In this sense, the formation of Car_{D1}^+ is advantageous not only to inhibit formation of $P680^{+\bullet}$ but also to facilitate charge recombination with Q_A^- directly via $P680^0Car^+Q_A^-$. If Q_A^- in the charge state $P680^0Car^+Q_A^-$ is in the high-potential form [58,63,64], the charge recombination via $P680^0Car^+Q_A^-$ can be more favorable than via $P680^{+\bullet}Pheo_{D1}^-$, since under these circumstances backward ET from Q_A^- to $Pheo_{D1}$ becomes inefficient because of the increase of the E_m difference between Q_A and $Pheo_{D1}$. The exact mechanism of formation of high-potential Q_A is unclear, although we recently found that formation of a $Q_A^{0/-}$-dependent H bond donated by the hydroxyl group of D2-Thr217 increases $E_m(Q_A)$ by 100 mV [65] and might thus contribute to the formation of high-potential Q_A.

3.5. Cluster of Car near Car_{D1}

From the new PSII structure, it became evident that Car_{D1} is surrounded by a number of Trp residues as formerly suggested for Car_{D2} [66]. For Car_{D1}, these residues are D1-Trp20, D1-Trp105, CP47-Trp75 with edge-to-edge distances of 4.2 Å, 3.5 Å, 4.2 Å, respectively and for Car_{D2} it is D2-Trp104 with an edge-to-edge distance of 4.0 Å.

A cluster of four Car (Car-103, Car-104, Car-105 and Car-106) connects Car_{D1} at the PSII monomer with the antenna Chl*a* in CP47 of the adjacent monomer (Fig. 1b). Except for Car-105 (E_m(Car-105)=+1124 mV) that is approximately parallel to the membrane plane, the calculated values of E_m for Car-103, Car-104 and Car-106 of +1043 mV, +1005 mV and +971 mV, respectively, (see Table 1) are at the same level as that calculated for Car_{D1} (+997 mV). Car-103 and Car-104 are in van der Waals contact, whereas Car-106 is separate from any other Car, but in van der Waals contact with Chl*a*-29 axially coordinated by CP47-His114 in the adjacent PSII monomer. This Chl*a* has been suggested to absorb at the significantly longer wavelength of 690 nm compared with 680 nm for P680 [67].

A direct charge recombination of $Car_{D1}^+Q_A^-$ (edge-to-edge distance 23 Å and π–π distance 25 Å) might be possible, but charge recombination of $Car\text{-}104^+Q_A^-$ might occur with higher yield on account of the proximity of Q_A to Car-104 (edge-to-edge distance 16 Å and π–π distance 17 Å). Unlike the axis of Car_{D1}, which is orthogonal to the membrane plane, that of Car-104 is oriented more parallel to the membrane plane. Furthermore, in contrast to Car_{D1}, Car-104 has a negatively charged SQDG-12 lipid in its neighborhood and is not surrounded by Trp. In terms of distances to Q_A, Car-104 is more likely Car_X than Car_{D1}. However, because of the similarity of the calculated E_m of +997 mV for Car_{D1} and of +1005 mV for Car-104, there is no indication of a large energy barrier for ET between the two Car and it is not clear at which Car the cationic charge state is localized. It should be noted that, except for photo-damaged PSII, the population of Car^+ is unlikely to increase because of efficient ET from the Mn-cluster to $P680^{+\bullet}$. Therefore, Car^+ is essentially absent in functional PSII and charge recombination of $Car^+Q_A^-$ is not competitive with the forward ET from Q_A^- to Q_B. Hence, it will be difficult to measure charge recombination of $Car^+Q_A^-$ in PSII RC directly. Lack of such experimental data precludes definite conclusions on the origin of the Car^+/Q_A^- state observed in the PSII enriched membranes [5].

4. Conclusion

The present PSII crystal structure at 3.0 Å resolution confirms the existence of Car_{D1} near $Chl_{Z(D1)}$ [18]. Both Car_{D1} in the PSII dimer are surrounded by another four Car and several lipid molecules. The calculated $E_m(Car_{D1})$ is as high as those of $Chl_{Z(D1)}$ and the nearby Car-104. On account of the wire-like shape of Car, Car-104 is also not too far from Q_A, at an edge-to-edge distance of 16 Å from the Q_A head group. This implies that a direct charge recombination of $Car\text{-}104^+Q_A^-$ without involving the $P680^{+\bullet}Pheo_{D1}^-$ charge state might be possible. The calculated values of E_m for Car and Chl_Z on the D2 side are lower than those on the D1 side. Furthermore, the calculated $E_m(Chl_{Z(D2)})$ is by lower 200 mV than $E_m(Car_{D2})$. These differences in E_m values are attributed to the specificity of the Mn-cluster and its surrounding titratable residues.

Generally, long-distance ET processes in proteins occur with small electronic coupling and therefore occur on the *electronically* non-adiabatic (but *vibronically* adiabatic) potential-energy surface, which comprises the diabatic energy surfaces of electron donor and acceptor moiety. The combined electronic and vibrational coupling between donor and acceptor sides are as important as the driving force (i.e. E_m difference between donor and acceptor) in determining the ET kinetics. Geometries of cofactors revealed in the present 3.0 Å PSII structure [18] are well enough defined to estimate the electronic couplings with empirical equations (for instance, see [68,69]). Information about vibrational modes can be obtained from the spectra of those molecules, if they are detectable. The present study provides E_m values for donor and acceptor sites involved in the ET event. From the electrostatic point of view, we consider the specificity of the Mn-cluster and its surrounding acidic residues as the principal reason that Car_{D2}^+ and $Chl_{Z(D2)}^+$ are preferentially observed in spectroscopic studies [5].

Acknowledgments

We thank Dr. Donald Bashford and Dr. Martin Karplus for providing the programs MEAD and CHARMM22, respectively. We thank Dr. Eberhard Schlodder, Dr. Frank Müh and Dr. Gary W. Brudvig for helpful discussions. We thank Dr. Dennis Diestler for critical reading of the manuscript. This work was supported by Deutsche Forschungsgemeinschaft SFB 498, Projects A4, A5, C7 Forschergruppe Project KN 329/5-1/5-2, GRK 80/2, GRK 268, GRK 788/1.

Appendix A. Supplementary data

Supplementary data associated with this article can be found, in the online version, at doi:10.1016/j.bbabio.2006.10.006.

References

[1] T.M. Bricker, The structure and function of CPa-1 and CPa-2 in photosystem II, Photosynth. Res. 24 (1990) 1–13.
[2] M.L. Groot, N.P. Pawlowicz, L.J.G.W. van Wilderen, J. Breton, I.H.M. van Stokkum, R. van Grondelle, Initial electron donor and acceptor in isolated photosystem II reaction centers identified with femtosecond mid-IR spectroscopy, Proc. Natl. Acad. Sci. U. S. A. 102 (2005) 13087–13092.
[3] L.K. Thompson, G.W. Brudvig, Cytochrome b-559 may function to protect photosystem II from photoinhibition, Biochemistry 27 (1988) 6653–6658.
[4] J. Hanley, Y. Deligiannakis, A. Pascal, P. Faller, A.W. Ruthrtford, Carotenoid oxidation in photosystem II, Biochemistry 38 (1999) 8189–8195.
[5] P. Faller, A. Pascal, A.W. Rutherford, b-carotene redox reactions in photosystem II: electron transfer pathway, Biochemistry 40 (2001) 6431–6440.
[6] R.J. van Dorssen, J. Breton, J.J. Plijter, K. Satoh, H.J. van Gorkom, J. Amesz, Spectroscopic properties of the reaction center and of the 47 kDa chlorophyll protein of photosystem II, Biochim. Biophys. Acta. 893 (1987) 267–274.
[7] S.L.S. Kwa, W.R. Newell, R. van Grondelle, J.P. Dekker, The reaction center of photosystem II studied with polarized fluorescence spectroscopy, Biochim. Biophys. Acta. 1099 (1992) 193–202.
[8] T. Tomo, M. Mimuro, M. Iwaki, M. Kobayashi, S. Itoh, K. Satoh, Topology of pigments in the isolated photosystem II reaction center studied by selective extraction, Biochim. Biophys. Acta. 1321 (1997) 21–30.
[9] A. Telfer, What is b-carotene doing in the photosystem II reaction centre? Philos. Trans. R. Soc. London B 357 (2002) 1431–1440.
[10] A. Telfer, D. Frolov, J. Barber, B. Robert, A. Pascal, Oxidation of the two b-carotene molecules in the photosystem II reaction center, Biochemistry 42 (2003) 1008–1015.
[11] C.A. Tracewell, G.W. Brudvig, Two redox-active b-carotene molecule in photosystem II, Biochemistry 42 (2003) 9127–9136.
[12] C.A. Tracewell, A. Cua, D.F. Bocian, G.W. Brudvig, Resonance Raman spectroscopy of carotenoids in photosystem II core complexes, Photosynth. Res. 83 (2005) 45–52.
[13] C.A. Tracewell, J.S. Vrettos, J.A. Bautista, H.A. Frank, G.W. Brudvig, Carotenoid photooxidation in photosystem II, Arch. Biochem. Biophys. 385 (2001) 61–69.
[14] J.A. Bautista, C.A. Tracewell, E. Schlodder, F.X.J. Cunningham, G.W. Brudvig, B.A. Diner, Construction and characterization of genetically modified Synechocystis sp. PCC 6803 photosystem II core complexes containing carotenoids with shorter p-conjugation than b-carotene, J. Biol. Chem. 280 (2005) 38839–38850.
[15] A. Zouni, H.T. Witt, J. Kern, P. Fromme, N. Krauß, W. Saenger, P. Orth, Crystal structure of photosystem II from *Synechococcus elongatus* at 3.8 Å resolution, Nature 409 (2001) 739–743.
[16] N. Kamiya, J.-R. Shen, Crystal structure of oxygen-evolving photosystem II from *Thermosynechococcus vulcanus* at 3.7-Å resolution, Proc. Natl. Acad. Sci. U. S. A. 100 (2003) 98–103.
[17] K.N. Ferreira, T.M. Iverson, K. Maghlaoui, J. Barber, S. Iwata, Architecture of the photosynthetic oxygen-evolving center, Science 303 (2004) 1831–1838.
[18] B. Loll, J. Kern, W. Saenger, A. Zouni, J. Biesiadka, Towards complete cofactor arrangement in the 3.0 Å resolution structure of photosystem II, Nature 438 (2005) 1040–1044.
[19] J. Kern, B. Loll, C. Luneberg, D. DiFiore, J. Biesiadka, K.-D. Irrgang, A. Zouni, Purification, characterisation and crystallisation of photosystem II from *Thermosynechococcus elongatus* cultivated in a new type of photobioreactor, Biochim. Biophys. Acta. 1706 (2005) 147–157.
[20] J. Yano, J. Kern, K.D. Irrgang, M.J. Latimer, U. Bergmann, P. Glatzel, Y. Pushkar, J. Biesiadka, B. Loll, K. Sauer, J. Messinger, A. Zouni, V.K. Yachandra, X-ray damage to the Mn4Ca complex in single crystals of photosystem II: a case study for metalloprotein crystallography, Proc. Natl. Acad. Sci. U. S. A. 102 (2006) 12047–12052.
[21] J. Biesiadka, B. Loll, J. Kern, K.-D. Irrgang, A. Zouni, Crystal structure of cyanobacterial photosystem II at 3.2 Å resolution: a closer look at the Mn-cluster, Phys. Chem. Chem. Phys. 6 (2004) 4733–4736.
[22] B.R. Brooks, R.E. Bruccoleri, B.D. Olafson, D.J. States, S. Swaminathan, M. Karplus, CHARMM: a program for macromolecular energy minimization and dynamics calculations, J. Comp. Chem. 4 (1983) 187–217.
[23] H. Ishikita, W. Saenger, J. Biesiadka, B. Loll, E.-W. Knapp, How photosynthetic reaction centers control oxidation power in chlorophyll pairs P680, P700 and P870, Proc. Natl. Acad. Sci. U. S. A. 103 (2006) 9855–9860.
[24] H. Ishikita, E.-W. Knapp, Redox potential of quinones in both electron transfer branches of photosystem I, J. Biol. Chem. 278 (2003) 52002–52011.
[25] C.I. Bayly, P. Cieplak, W.D. Cornell, P.A. Kollman, A well-behaved electrostatic potential based method using charge restraints for deriving atomic charges: the RESP model, J. Phys. Chem. 97 (1993) 10269–10280.
[26] Jaguar4.2, (1991–2000) Schrödinger, Inc., Portland, OR.
[27] A.D. MacKerell Jr., D. Bashford, R.L. Bellott, R.L. Dunbrack Jr., J.D. Evanseck, M.J. Field, S. Fischer, J. Gao, H. Guo, S. Ha, D. Joseph-McCarthy, L. Kuchnir, K. Kuczera, F.T.K. Lau, C. Mattos, S. Michnick, T. Ngo, D.T. Nguyen, B. Prodhom, W.E. Reiher III, B. Roux, M. Schlenkrich, J.C. Smith, R. Stote, J. Straub, M. Watanabe, J. Wiorkiewicz-Kuczera, D. Yin, M. Karplus, All-atom empirical potential for molecular modeling and dynamics studies of proteins, J. Phys. Chem., B 102 (1998) 3586–3616.
[28] D. Bashford, M. Karplus, pKa's of ionizable groups in proteins: atomic detail from a continuum electrostatic model, Biochemistry 29 (1990) 10219–10225.
[29] C. Tommos, X.-S. Tang, K. Warncke, C.W. Hoganson, S. Styring, J. McCracken, B.A. Diner, G.T. Babcock, Spin-density distribution, conformation, and hydrogen bonding of the redox-active tyrosine YZ in photosystem II from multiple-electron magnetic-resonance spectroscopies: implications for photosynthetic oxygen evolution, J. Am. Chem. Soc. 117 (1995) 10325–10335.
[30] M. Haumann, A. Mulkidjanian, W. Junge, Tyrosine-Z in oxygen-evolving photosystem II: a hydrogen-bonded tyrosinate, Biochemistry 38 (1999) 1258–1267.
[31] J.A. Jeevarajan, L.D. Kispert, Electrochemical oxidation of carotenoids containing donor/acceptor substituents, J. Electroanal. Chem. 411 (1996) 57–66.
[32] P. Hapiot, L.D. Kispert, V.V. Konovalov, J.-M. Saveant, Single two-electron transfers vs. successive one-electron transfers in polyconjugated systems illustrated by the electrochemical oxidation and reduction of carotenoids, J. Am. Chem. Soc. 123 (2001) 6669–6677.
[33] H. Ishikita, E.-W. Knapp, Redox potentials of chlorophylls and β-carotene in the antenna complexes of photosystem II, J. Am. Chem. Soc. 127 (2005) 1963–1968.
[34] T. Watanabe, M. Kobayashi, Electrochemistry of chlorophylls, in Chlorophylls, in: H. Scheer (Ed.), CRC Press, Boca Raton, FL., 1991, pp. 287–303.
[35] J. Fajer, I. Fujita, M.S. Davis, A. Forman, L.K. Hanson, K.M. Smith, Photosynthetic energy transduction: spectral and redox characteristics of

chlorophyll radicals in vitro and in vivo, in electrochemical and spectrochemical studies of biological redox components, in: K.M. Kadish (Ed.), American chemical society, Washington, D. C, 1982, chapter 21.
[36] L.L. Maggiora, J.D. Petke, D. Gopal, R.T. Iwamoto, G.M. Maggiora, Experimental and theoretical studies of Schiff basechlorophylls, Photochem. Photobiol. 42 (1985) 69–75.
[37] Y. Sugita, N. Miyashita, M. Ikeguchi, A. Kidera, C. Toyoshima, Protonation of the acidic residues in the transmembrane cation-binding sites of the Ca^{2+} pump, J. Am. Chem. Soc. 127 (2005) 6150–6151.
[38] D.H. Stewart, A. Cua, D.A. Chisholm, B.A. Diner, D.F. Bocian, G.W. Brudvig, Identification of histidine 118 in the D1 polypeptide of photosystem II as the axial ligand to chlorophyll Z, Biochemistry 37 (1998) 10040–10046.
[39] K.V. Lakshmi, O.G. Poluektov, M.J. Reifler, A.M. Wagner, M.C. Thurnauer, G.W. Brudvig, Pulsed high-frequency EPR study on the location of carotenoid and chlorophyll cation radicals in photosystem II, J. Am. Chem. Soc. 125 (2003) 5005–5014.
[40] M. Roncel, A. Boussac, J.L. Zurita, H. Bottin, M. Sugiura, D. Kirilovsky, J.M. Ortega, Redox properties of the photosystem II cytochromes b559 and c550 in the cyanobacterium *Thermosynechococcus elongatus*, J. Biol. Inorg. Chem. 8 (2003) 206–216.
[41] J. Wang, D. Gosztola, S.V. Ruffle, C. Hemann, M. Seibert, M.R. Wasielewski, R. Hille, T.L. Gustafson, R.T. Sayre, Functional asymmetry of photosystem II D1 and D2 peripheral chlorophyll mutants of *Chlamydomonas reinhardtii*, Proc. Natl. Acad. Sci. U. S. A. 99 (2002) 4091–4096.
[42] C.A. Tracewell, A. Cua, D.H. Stewart, D.F. Bocian, G.W. Brudvig, Characterization of carotenoid and chlorophyll photooxidation in photosystem II, Biochemistry 40 (2001) 193–203.
[43] A. Kawamori, T.-A. Ono, A. Ishii, S. Nakazawa, H. Hara, T. Tomo, J. Minagawa, R. Bittl, S.A. Dzuba, The functional sites of chlorophylls in D1 and D2 subunits of Photosystem II identified by pulsed EPR, Photosynth. Res. 84 (2005) 187–192.
[44] S. Vasil'ev, G.W. Brudvig, D. Bruce, The X-ray structure of photosystem II reveals a novel electron transport pathway between P680, cytochrome b_{559} and the energy-quenching cation, Chl_Z^+, FEBS Lett. 543 (2003) 159–163.
[45] H. Ishikita, E.W. Knapp, Function of redox-active tyrosine in photosystem II, Biophys. J. 90 (2006) 3886–3896.
[46] P. Sebban, P. Maróti, M. Schiffer, D.K. Hanson, Electrostatic dominoes: long distance propagation of mutational effects in photosynthetic reaction centers of *Rhodobacter capsulatus*, Biochemistry 34 (1995) 8390–8397.
[47] H.L. Axelrod, E.C. Abresch, M.L. Paddock, M.Y. Okamura, G. Feher, Determination of the binding sites of the proton transfer inhibitors Cd^{2+} and Zn^{2+} in bacterial reaction centers, Proc. Natl. Acad. Sci. U. S.A. 97 (2000) 1542–1547.
[48] H. Ishikita, E.-W. Knapp, Induced conformational change upon Cd^{2+} binding at photosynthetic reaction centers, Proc. Natl. Acad. Sci. U. S. A. 102 (2005) 16215–16220.
[49] S. Iwata, J. Barber, Structure of photosystem II and molecular architecture of the oxygen-evolving centre, Curr. Opin. Struct. Biol. 14 (2004) 447–453.
[50] J. Barber, K. Ferreira, K. Maghlaoui, S. Iwata, Structural model of the oxygen-evolving centre of photosystem II with mechanistic implications, Phys. Chem. Chem. Phys. 6 (2004) 4737–4742.
[51] J. De Las Rivas, J. Barber, Analysis of the structure of the PsbO protein and its implications, Photosynth. Res. 81 (2004) 329–343.
[52] H. Ishikita, W. Saenger, B. Loll, J. Biesiadka, E.-W. Knapp, Energetics of a possible proton exit pathway for water oxidation in photosystem II, Biochemistry 45 (2006) 2063–2071.
[53] J. De Las Rivas, A. Telfer, J. Barber, Two coupled β-carotene molecules protect P680 from photodamage in isolated photosystem II reaction centres, Biochim. Biophys. Acta. 1142 (1993) 155–164.
[54] T. Noguchi, T. Tomo, Y. Inoue, Fourier transform infrared study of the cation radical of P680 in the photosystem II reaction center: evidence for charge delocalization on the chlorophyll dimer, Biochemistry 37 (1998) 13614–13625.
[55] D. Zheleva, J. Sharma, M. Panico, H.R. Morris, J. Barber, Isolation and characterization of monomeric and dimeric CP47-reaction center photosystem II complexes, J. Biol. Chem. 273 (1998) 16122–16127.
[56] M. Bianchetti, D. Zheleva, Z. Deak, S. Zharmuhamedov, V. Klimov, J.H.A. Nugent, I. Vass, J. Barber, Comparison of the functional properties of the monomeric and dimeric forms of the isolated CP47-reaction center complex, J. Biol. Chem. 273 (1998) 16128–16133.
[57] C. Büchel, J. Barber, G. Ananyev, S. Eshaghi, R. Watt, C. Dismukes, Photoassembly of the manganese cluster and oxygen evolution from monomeric and dimeric CP47 reaction center photosystem II complexes, Proc. Natl. Acad. Sci. U. S. A. 96 (1999) 14288–14293.
[58] G.N. Johnson, A.W. Rutherford, A. Krieger, A change in the midpoint potential of the quinone QA in photosystem II associated with photoactivation of oxygen evolution, Biochim. Biophys. Acta. 1229 (1995) 202–207.
[59] Y. Takahashi, Ö. Hansson, P. Mathis, K. Satoh, Primary radical pair in the photosystem II reaction centre, Biochim. Biophys. Acta. 893 (1987) 49–59.
[60] J.R. Durrant, L.B. Giorgi, J. Barber, D.R. Klug, G. Porter, Characterisation of triplet states in isolated photosystem II reaction centres: oxygen quenching as a mechanism for photodamage, Biochim. Biophys. Acta 1017 (1990) 167–175.
[61] J. Barber, M.D. Archer, P680, the primary electron donor of photosystem II, J. Photochem. Photobiol., A Chem. 142 (2001) 97–106.
[62] R. de Wijn, H.J. van Gorkom, The rate of charge recombination in photosystem II, Biochim. Biophys. Acta. 1553 (2002) 302–308.
[63] A. Krieger, E. Weis, Energy dependent quenching of chlorophyll α fluorescence: the involvement of proton–calcium exchange at photosystem II, Photosynthetica 27 (1992) 89–98.
[64] A. Krieger, A.W. Rutherford, G.N. Johnson, On the determination of redox midpoint potential of the primary quinone electron transfer acceptor, Q_A, in photosystem II, Biochim. Biophys. Acta 1229 (1995) 193–201.
[65] H. Ishikita, E.-W. Knapp, Control of quinone redox potentials in photosystem II: electron transfer and photoprotection, J. Am. Chem. Soc. 127 (2005) 14714–14720.
[66] Y. Deligiannakis, J. Hanley, A.W. Rutherford, Carotenoid oxidation in photosystem II: 1D- and 2D-electron spin-echo envelope modulation study, J. Am. Chem. Soc. 122 (2000) 400–401.
[67] G. Shen, W.F.J. Vermaas, Mutation of chlorophyll ligands in the chlorophyll-binding CP47 protein as studied in a Synechocystis sp. PCC 6803 photosystem I-less background, Biochemistry 33 (1994) 7379–7388.
[68] C.C. Moser, J.M. Keske, F. Warncke, R.S. Farid, P.L. Dutton, Nature of biological electron transfer, Nature 355 (1992) 796–802.
[69] C.C. Page, C.C. Moser, X. Chen, P.L. Dutton, Natural engineering principles of electron tunnelling in biological oxidation-reduction, Nature 402 (1999) 47–52.